THE JOURNAL OF PHYSICAL CHEMISTRY C

Article

Cite This: J. Phys. Chem. C 2018, 122, 26298−26306

pubs.acs.org/JPCC

Concentration Quenching in Upconversion Nanocrystals

Zijun Wang and Andries Meijerink*

Condensed Matter and Interfaces, Debye Institute for Nanomaterials Science, Utrecht University, Princetonplein 1, 3584 CC Utrecht, Netherlands

Supporting Information

ABSTRACT: Despite considerable effort to improve upconversion (UC) in lanthanide-doped nanocrystals (NCs), the maximum reported efficiencies remain below 10%. Recently, we reported on low Er^{3+}- and Yb^{3+}-doped $NaYF_4$ NCs giving insight into fundamental processes involved in quenching for isolated ions. In practice, high dopant concentrations are required and there is a trend toward bright UC in highly doped NCs. Here, additional quenching processes due to energy transfer and migration add to a reduction in UC efficiency. However, a fundamental understanding on how concentration quenching affects the quantum efficiency is lacking. Here, we report a systematic investigation on concentration-dependent decay dynamics for Er^{3+} or Yb^{3+} doped at various concentrations (1−100%) in core and core−shell $NaYF_4$ NCs. The qualitative and quantitative analyses of luminescence decay curves and emission spectra show strong concentration quenching for the green-emitting Er^{3+} $^4S_{3/2}$ and NIR-emitting $^4I_{11/2}$ levels, whereas concentration quenching for the red-emitting $^4F_{9/2}$ level and the IR-emitting $^4I_{13/2}$ level is limited. The NIR emission of Yb^{3+} remains efficient even at concentration as high as 60% Yb^{3+}, especially in core−shell NCs. Finally, the role of solvent quenching was investigated and reveals a much stronger quenching in aqueous media that can be explained by the high-energy O−H vibrations. The present study uncovers a more complete picture of quenching processes in highly doped UC NCs and serves to identify methods to further optimize the efficiency by careful tuning of lanthanide concentrations and core−shell design.

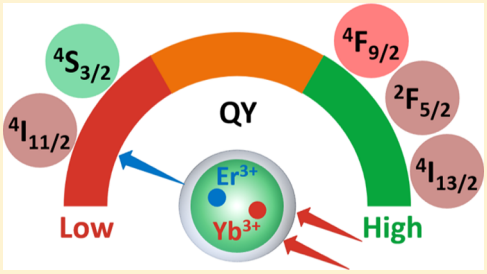

INTRODUCTION

Upconversion (UC) luminescence has become an active field of research since the pioneering work by Auzel, Ovsyankin, and Feofilov in 1960s. Especially in the past two decades, the advent of UC nanocrystals (NCs) has triggered renewed interests by emerging applications of UC NCs in bioimaging, solar cells, sensors, anticounterfeiting, and three-dimensional (3D) displays.[1−5] Upconverting two (or more) low-energy photons to one high-energy photon has been demonstrated for a variety of combinations of lanthanide ions and in different spectral regions, ranging from IR → NIR UC to vis → UV UC.[1−8] The Yb^{3+}−Er^{3+} ion couple is one of the most efficient UC couples showing efficient conversion of NIR (∼980 nm) to green and red light.[7,9] The intensity ratio of green and red emission can be tuned by varying experimental parameters, such as host matrix, dopant concentration, excitation power, dispersion medium, and size of NCs.[3] Trivalent Er^{3+} ion without a sensitizer also shows NIR-to-green UC, although less efficient, by excitation at 980 nm.[10] Also, an efficient IR (1520 nm)-to-NIR (980 nm) conversion has been reported for Er^{3+}.[11]

In spite of the great potential of UC materials, applications are often hampered by the low quantum yield (QY), especially in NCs. The UC QY in NCs is typically below a few percent, in spite of approaches aimed at enhancing the efficiency, including surface passivation, shell growth, broadband sensitization, and photonic and plasmonic engineering.[12] Recently reported strategies of incorporating high dopant concentrations combined with increased excitation densities have shown superior UC brightness. The explanation is the enhanced absorption (related to higher concentrations of absorbing ions) and the quadratic dependence of UC rates on excitation power and dopant concentration. All of these factors cause the UC to rapidly gain importance over other processes, such as quenching and IR emission from intermediate levels that do not have a quadratic power/concentration dependence.[13,14] The extreme brightness of UC in highly doped UC NCs under high power density excitation is promising, but it is crucial for many applications to reduce the excitation power to prevent heating and allow for safe operation conditions. Therefore, it is important to quantify and understand the underlying additional (concentration) quenching mechanisms in highly doped UC NCs to realize high UC brightness under reduced excitation densities. Recently, progress has been made in reducing excitation powers for single-NC experiments by optimizing Yb and Er concentrations and single UC NC imaging was reported in highly doped $NaYF_4$ core−shell NCs at excitation powers below 10 W/cm^2.[15,16]

The efficiency of UC NCs is lower than that in bulk materials. One reason is the surface-related quenching by defects, surface ligands, and surrounding solvent molecules with high-energy vibrational modes.[17,18] These quenching

Received: September 25, 2018
Revised: October 19, 2018
Published: October 19, 2018

DOI: 10.1021/acs.jpcc.8b09371
J. Phys. Chem. C 2018, 122, 26298−26306

mechanisms are especially pronounced for dopants on or near the NC surface. Coating of an inert (undoped) shell can effectively isolate the optically active lanthanide ions from the surface and surrounding energy vibrations to reduce surface quenching.[19−22] Recently, our group has established a model that accurately models solvent quenching for isolated lanthanide ions in UC NCs.[23] In this model, low dopant concentrations of Er^{3+} or Yb^{3+} were used to quantitatively describe and understand the quenching processes involved for individual dopant ions inside the NC. However, since UC relies on multistep energy transfer (ET), high dopant concentrations are crucial to realize efficient ET between lanthanide neighbors to enhance the UC efficiency. On the other hand, the high density of dopants opens additional channels for quenching and thus efficiency loss by concentration quenching via nonradiative processes, such as energy migration and cross-relaxation.[24−27] The trade-off between efficiency loss by concentration quenching and efficiency gain by ET UC determines the maximum UC QY. In addition, the higher absorption strength for higher dopant concentrations results in higher brightness, even at reduced QYs.

In spite of the various studies on UC in highly doped NCs, the role of concentration quenching in UC NCs is still not well understood and is not easy to model. To gain insight into the role of quenching processes at high dopant concentrations, here, we present a systematic investigation on the concentration dependence of UC dynamics of respective Er^{3+} and Yb^{3+} excited states for core and core−shell $NaYF_4$ NCs doped with 1−100% Er^{3+} or Yb^{3+}. Luminescence spectra and lifetime measurements under direct excitation in the emitting level are reported and analyzed to quantify concentration quenching for individual levels involved in UC processes. The results demonstrate that concentration quenching varies for different emitting levels and reveal how it is suppressed in core−shell NCs, e.g., the Er^{3+} $^4I_{11/2}$ NIR level is highly susceptible to concentration quenching even in core−shell NCs, whereas for Yb^{3+} in core−shell NCs, concentration quenching is very limited. Finally, the role of solvent quenching was investigated and reveals the role of UC quenching in NCs due to coupling with high-energy vibrations of the solvent. The present results give insight on the role of ET processes in the quenching of emission for energy levels of Er^{3+} and Yb^{3+} involved in IR to vis UC in NCs and provide design rules for highly doped NCs with improved UC quantum efficiencies.

RESULTS AND DISCUSSION

Concentration Quenching for UC NCs. *Characterization of NCs.* The Yb^{3+}−Er^{3+} ion couple is widely used to upconvert IR radiation through ground state absorption by two Yb^{3+} ions followed by a two-step ET to an Er^{3+} neighbor. $NaYF_4$:Yb,Er is an efficient UC material that serves as a model system both for bulk (microcrystalline) and nanocrystalline materials. In the present study, we analyze $NaYF_4$ core NCs that are singly doped with 1−100% Er^{3+} or Yb^{3+}. In addition, we investigate the influence of an inert 5 nm $NaYF_4$ shell coated on a selection of concentrations (1, 10, and 60%) of Er^{3+}- or Yb^{3+}-doped core NCs. These three concentrations are selected to represent NCs with limited interaction between dopant ions (low concentration, 1%), ET between neighboring ions but with no energy migration (intermediate concentration, 10%), and a concentration above the percolation point allowing for 3D energy migration (high concentration, 60%). This allows to distinguish between two types of energy transfer: energy migration (involving energy transfer among dopants to the same excited state of identical neighboring ions), which in principle does not lead to quenching or shortening of the lifetime because the excited-state population of the level involved does not change. However, it can induce quenching by diffusion (multiple ET steps) of the excited state from ions in the center (no quenching sites nearby) to identical ions at the surface (close to quenching sites) where quenching occurs. This will result in a faster decay time for high doping concentrations, typically above 10% because multistep energy transfer is need. The second type of energy transfer is cross-relaxation, which depopulates the excited state by partial energy transfer to a neighboring ion. This directly quenches the excited state and shortens the decay time and is already observed at lower doping concentrations.

Details on synthesis are in the Supporting Information (SI). First, we focus on the Er^{3+}-doped NCs. Figure 1a,b shows the representative transmission electron microscopy (TEM) images for monodisperse $NaYF_4$:1% Er^{3+} core (25 × 18 nm) and $NaYF_4$:1% Er^{3+}@$NaYF_4$ core−shell (35 × 28 nm) NCs. At higher Er^{3+} doping concentrations, the size and morphology of NCs are maintained (Figure S1). The 5 nm thick inert shell helps to suppress but will not fully eliminate surface quenching.[22,23,28]

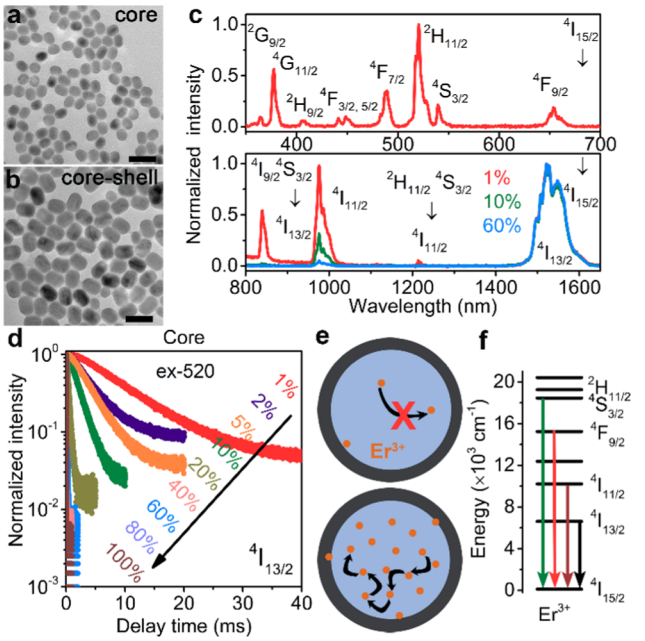

Figure 1. TEM images of (a) $NaYF_4$:1% Er^{3+} core and (b) $NaYF_4$:1% Er^{3+}@$NaYF_4$ core−shell NCs (scale bar = 50 nm). (c) Excitation spectrum of $NaYF_4$:1% Er^{3+}@$NaYF_4$ core−shell NCs for 1522 nm emission and emission spectra of $NaYF_4$:*X*% Er^{3+}@$NaYF_4$ core−shell NCs (*X* = 1, 10, and 60) for 520 nm excitation. (d) Luminescence decay curves of $^4I_{13/2}$ emission excited at 520 nm for $NaYF_4$:*X*% Er^{3+} core NCs (*X* = 1−100). (e) Schematic illustration of interaction between Er^{3+} ions for low and high concentrations of Er^{3+}. (f) Energy-level diagram of Er^{3+} showing emission (colored arrows) from levels studied in this work.

First, the optical properties were analyzed by recording luminescence spectra. Figure 1c shows the emission and excitation spectra for Er^{3+}-doped core−shell NCs. The excitation lines at 377, 489, 520, 540, and 654 nm are assigned to characteristic Er^{3+} transitions from the $^4I_{15/2}$ ground state to

DOI: 10.1021/acs.jpcc.8b09371
J. Phys. Chem. C 2018, 122, 26298−26306

the $^4G_{11/2}$, $^4F_{7/2}$, $^2H_{11/2}$, $^4S_{3/2}$, and $^4F_{9/2}$ states. The emission spectrum in the lower panel of Figure 1c recorded for $^2H_{11/2}$ excitation (520 nm) shows that, in addition to emission in the visible (green $^4S_{3/2}$ and red $^4F_{9/2}$ emission, not shown), the NCs emit in the IR at 840 ($^4I_{9/2} \rightarrow {}^4I_{15/2}$ and $^4S_{3/2} \rightarrow {}^4I_{13/2}$), 976 ($^4I_{11/2} \rightarrow {}^4I_{15/2}$), and 1522 nm ($^4I_{13/2} \rightarrow {}^4I_{15/2}$). It is clearly observed in the emission spectra that upon increasing the Er^{3+} concentration, the relative emission intensities from levels higher than $^4I_{13/2}$ decrease by concentration quenching. In core-only NCs, emission from each excited state, including the $^4I_{13/2}$ state, is quenched for higher dopant concentrations because of stronger surface-related quenching. Quenching of emission can be accurately probed by luminescence decay measurements. With a fixed radiative decay rate, the presence of additional nonradiative (quenching) pathways will result in a faster decay. As an example, in Figure 1d, the luminescence decay curves of the $^4I_{13/2}$ emission are shown for increasing Er^{3+} concentrations in core-only NCs. Significant quenching is observed, especially for concentrations higher than 10%, when long-range energy migration becomes possible. To reduce quenching, an inert shell[18,21] is grown on the selection of cores with 1, 10, and 60% Er^{3+}. The actual Er^{3+} concentrations incorporated in the NCs are verified by inductively coupled plasma (ICP) analysis. The results in Table S1 show that these concentrations in the NCs are close to the nominally added concentrations. In Figure 1e, the ET processes for the two extreme concentrations are schematically indicated (1%, limited interaction/no ET between Er^{3+} ions and 60%, energy migration over a network of multiple Er^{3+} ions).

Luminescence Decay Dynamics for Er^{3+} IR-Emitting Levels. Luminescence decay curves provide important information on luminescence quenching processes. In the present study, we focus on the $^4S_{3/2}$, $^4F_{9/2}$, $^4I_{11/2}$, and $^4I_{13/2}$ excited states, which are all involved in UC processes (Figure 1f). The solvent used for all measurements (unless otherwise specified) is cyclohexane. We first consider the concentration dependence of the luminescence decay for the IR-emitting $^4I_{13/2}$ and $^4I_{11/2}$ excited states, which serve as intermediate levels for IR → NIR and NIR → vis UC.[29−31] Figure 2 shows the $^4I_{13/2}$ and $^4I_{11/2}$ decay dynamics after direct excitation in the emitting level for core and core−shell NCs with 1, 10, and 60% Er^{3+} in the core. There is a deviation from single-exponential decay, especially for Er^{3+} emission in core-only NCs. The initial fast decay is explained by faster quenching for near-surface Er^{3+} ions. Growth of a 5 nm protective shell reduces the initial fast decay. To obtain a better insight into the quenching of the emission, the luminescence decay is quantified by a lifetime obtained from single-exponential fitting and also by an average lifetime defined by $\sum_0^t tI(t)/\sum_0^t I(t)$, where $I(t)$ is the emission intensity at time t. The average lifetimes (indicated in the figures) are close to the values obtained from a single-exponential fitting. For core and core−shell NCs, the same trend is observed: the $^4I_{13/2}$ and $^4I_{11/2}$ emission lifetimes decrease as Er^{3+} concentration increases due to concentration quenching. However, the reduction in lifetime is much stronger in the core-only NCs, especially for high Er^{3+} concentrations. There is also a significant difference between concentration quenching observed for the $^4I_{13/2}$ and $^4I_{11/2}$ levels. Both emissions are strongly quenched in the core-only NCs. On the basis of the reduction in $^4I_{13/2}$ and $^4I_{11/2}$ lifetimes from over 1 ms (1% Er^{3+}) to ~80 μs (60% Er^{3+}) in the core-only NCs, it is evident

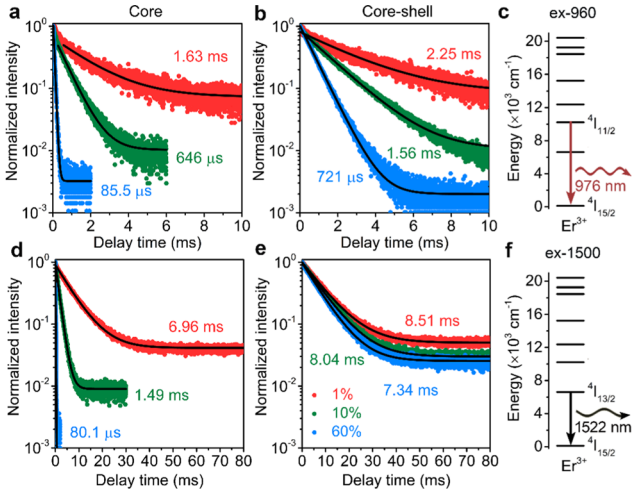

Figure 2. Luminescence decay curves of Er^{3+} $^4I_{11/2}$ ((a) core, (b) core−shell, and (c) corresponding energy-level diagram) and $^4I_{13/2}$ ((d) core, (e) core−shell, and (f) corresponding energy-level diagram) emission by direct excitation at 960 and 1500 nm for $NaYF_4$:*X*% Er^{3+} core and $NaYF_4$:*X*% Er^{3+}@$NaYF_4$ core−shell NCs (*X* = 1, 10, and 60 in red, green, and blue color).

that there is strong concentration quenching, giving rise to a quantum yield below 10% in core-only NCs. For the 1522 nm emission from the $^4I_{13/2}$ level, the lifetime increases upon growth of an inert shell and a lifetime of ~8 ms is observed, which is close to the radiative lifetime. The slight reduction from 8.51 (1% Er^{3+}) to 7.34 ms (60% Er^{3+}) reveals that the (concentration) quenching of the $^4I_{13/2}$ level is almost exclusively surface-related and can be successfully suppressed by shell growth. As a result, the absolute intensity of the $^4I_{13/2}$ emission increases in highly Er-doped core−shell NCs for excitation in higher-energy levels ($^4I_{11/2}$, $^4F_{9/2}$, or $^4S_{3/2}$) as relaxation to the $^4I_{13/2}$ level is enhanced by cross-relaxation and energy migration whereas the $^4I_{13/2}$ emission is not quenched upon increasing the Er-doping concentration.

The situation is different for the $^4I_{11/2}$ level. Shell growth reduces quenching, but still the decay time significantly changes in core−shell NCs upon raising the Er^{3+} concentration from 1 (2.25 ms) to 10 (1.56 ms) to 60% (721 μs). This difference indicates that for the $^4I_{11/2}$ level, in addition to surface quenching, additional quenching pathways contribute. In our recent paper,[23] we suggested a role of the high-energy (3300−3500 cm^{-1}) O−H vibrations, which are resonant with the $^4I_{11/2}$ to $^4I_{13/2}$ energy gap. It is hard to prevent the incorporation of OH^- groups on F^- lattice sites in view of their chemical similarity. The present observations are consistent with the presence of OH^- quenching centers inside the NC core. At higher Er^{3+} concentrations, energy migration to OH^- centers inside the core will occur, which reduces the luminescence efficiency and gives rise to faster luminescence decay even when quenching by surface sites is reduced by growth of an inert shell. For the emission from the $^4I_{13/2}$ level (with a larger ~6500 cm^{-1} energy gap to the ground state), quenching occurs through multiphonon relaxation at the surface, which can be effectively eliminated by shell growth, making the $^4I_{13/2}$ emission highly efficient (close to 100% QY) even at high (60%) Er^{3+} concentrations.

For comparison, we also measured the decay dynamics for $^4I_{13/2}$ and $^4I_{11/2}$ emissions after indirect excitation at 520 nm ($^4I_{15/2} \rightarrow {}^2H_{11/2}$, Figure S2). Because the $^4S_{3/2}/{}^2H_{11/2}$ state acts

DOI: 10.1021/acs.jpcc.8b09371
J. Phys. Chem. C 2018, 122, 26298−26306

as an energy reservoir that feeds the IR-emitting states through multiphonon relaxation, radiative decay, and cross-relaxation processes, a rise time can be observed. The rise time becomes shorter for higher Er^{3+} concentrations, resulting from faster ET and cross-relaxation.[32] Qualitatively, the influence of Er^{3+} concentration and shell growth on decay times after indirect (Figure S2) and direct (Figure 2) excitation is the same. However, the absolute values of the lifetimes are different and longer lifetimes are measured after indirect excitation and even can be longer than the radiative lifetime.[33] This makes it difficult to make a meaningful comparison of lifetimes and gain insight into the intrinsic luminescence quenching for the levels of Er^{3+} and Yb^{3+} involved in the UC. This illustrates that it is cumbersome to retrieve quantitative information on luminescence quenching for specific energy levels following excitation in higher (feeding) energy levels and shows the importance of analyzing luminescence decay curves following direct excitation in the emitting state.

Luminescence Decay Dynamics for Er^{3+} Vis-Emitting Levels. After ET UC, the higher-energy $^4S_{3/2}$ and $^4F_{9/2}$ states are populated and emit green and red UC emissions. It is also interesting to investigate efficiency losses related to concentration quenching for these emitting levels. Figure 3 shows the $^4S_{3/2}$ and $^4F_{9/2}$ decay dynamics as a function of Er^{3+} concentration under direct excitation. As for the IR-emitting levels, concentration quenching shortens the lifetime and the inert shell reduces the effect of concentration quenching. However, there are clear differences between the two levels. Upon increasing the Er^{3+} concentration, a much stronger quenching is observed for the green-emitting $^4S_{3/2}$ level than for the red-emitting $^4F_{9/2}$ level. This is explained by cross-relaxation[34] of $^4S_{3/2} + {}^4I_{15/2} \rightarrow {}^4I_{9/2} + {}^4I_{13/2}$ as an additional $^4S_{3/2}$ decay channel that becomes available at higher Er^{3+} concentrations and causes a more than 10-fold decrease in lifetime upon raising the Er^{3+} concentration from 1 to 10% (345−24 μs). In the literature, energy migration was suggested to be the mechanism of concentration quenching of the $^4S_{3/2}$ emission, excluding cross-relaxation.[33] The present results show pronounced quenching of the $^4S_{3/2}$ emission both in core and core−shell NCs already for 10% Er^{3+} where energy migration is limited. Efficient cross-relaxation quenching for Er^{3+} $^4S_{3/2}$ emission has been reported, both in bulk and nanocrystalline materials.[35] The strong contribution to cross-relaxation quenching is confirmed by lifetime measurements of the green Er^{3+} emission in the core−shell NCs. Shell growth reduces the quenching, but still a strong decrease of the decay time is observed from 436 (1% Er^{3+}) to 125 μs (10% Er^{3+}). This is a clear signature of cross-relaxation quenching and not surface-related quenching.

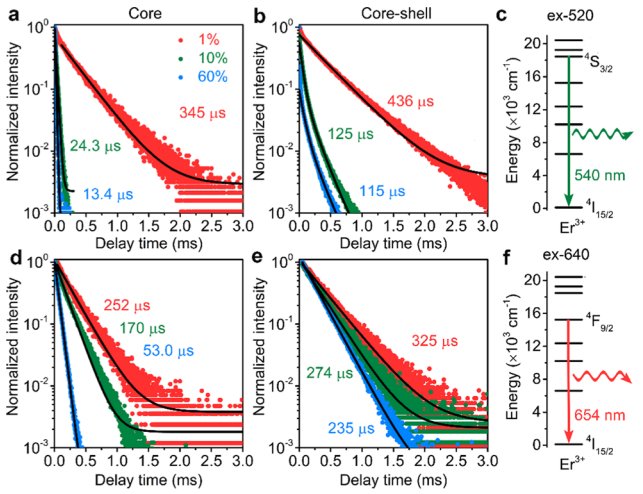

Figure 3. Luminescence decay curves of Er^{3+} $^4S_{3/2}$ ((a) core; (b) core−shell; (c) corresponding energy-level diagram) and $^4F_{9/2}$ ((d) core; (e) core−shell; (f) corresponding energy-level diagram) emissions by direct excitations of 520 and 640 nm for $NaYF_4$:*X*% Er^{3+} core and $NaYF_4$:*X*% Er^{3+}@$NaYF_4$ core−shell NCs (*X* = 1, 10, 60 in red, green, and blue color, respectively).

The luminescence decay curves for the red $^4F_{9/2}$ emission (Figure 3d,e) in core-only NCs show only limited quenching at 10% doping (decrease in lifetime from 252 to 170 μs). This is consistent with the fact that there is no resonant cross-relaxation path for the $^4F_{9/2}$ level. At 60% Er^{3+}, a stronger decrease in lifetime is observed (53 μs) that can be explained by energy migration to the surface where quenching occurs. Upon shell growth, surface quenching is suppressed and the $^4F_{9/2}$ emission lifetimes lengthen to values close to those in the 1% sample, showing that concentration quenching for the $^4F_{9/2}$ emission is very limited up to very high (60%) Er^{3+} concentrations in core−shell NCs.

On the basis of the results above, important information on the concentration quenching in highly Er^{3+}-doped $NaYF_4$ NCs can be obtained. Under low excitation powers, strong concentration quenching is observed for all emitting levels ($^4S_{3/2}$, $^4F_{9/2}$, $^4I_{11/2}$, and $^4I_{13/2}$) in core-only NCs with 60% Er^{3+}. The quenching for the $^4S_{3/2}$ (545 nm) and $^4I_{11/2}$ (976 nm) emission is stronger and is not only caused by surface quenching but also by cross-relaxation ($^4S_{3/2}$) and O−H vibrations ($^4I_{11/2}$) inside the NC core. Growth of an inert shell cannot eliminate these quenching pathways. For the $^4F_{9/2}$ (654 nm) and $^4I_{13/2}$ (1522 nm) levels, the dominant mechanism for concentration quenching is energy migration to the surface where multiphonon relaxation and possibly also surface defect states quench the emission. Growth of an inert shell (5 nm thickness here) can effectively eliminate these quenching processes and efficient red ($^4F_{9/2}$) or IR ($^4I_{13/2}$) emission is observed up to the highest Er^{3+} concentrations.

To analyze the concentration quenching for UC more quantitatively, we determined lifetime ratios for core and core−shell NCs for the three different Er^{3+} concentrations (1, 10, and 60%), as summarized in Table 1. The lifetime ratios for 1% Er^{3+}-doped core−shell and core NCs (1st row) are a measure for how well the 5 nm shell shields the respective levels from quenching by high-energy vibrations of the solvent/ligand. The ratios are similar (around 1.3) for the four different levels. This indicates that vibrational quenching

Table 1. Ratios of Emission Lifetimes for Various Levels of Er^{3+} ($^4S_{3/2}$, $^4F_{9/2}$, $^4I_{11/2}$, and $^4I_{13/2}$) and Yb^{3+} ($^2F_{5/2}$) Doped in Core-Only (τ_c) and Core−Shell (τ_{c-s}) NCs with Different Concentrations (1, 10, or 60%) of Er^{3+} or Yb^{3+}

	$^4S_{3/2}$	$^4F_{9/2}$	$^4I_{11/2}$	$^4I_{13/2}$	$^2F_{5/2}$
$\tau_{c-s/1\%}/\tau_{c/1\%}$	1.26	1.29	1.38	1.22	1.08
$\tau_{c-s/1\%}/\tau_{c-s/10\%}$		1.19	1.44	1.06	1.07
$\tau_{c-s/1\%}/\tau_{c-s/60\%}$		1.38	3.12	1.22	2.92
$\tau_{c-s/10\%}/\tau_{c-s/60\%}$		1.17	2.16	1.16	2.72
$\tau_0/\tau_{c-s/1\%}$	1.66	1.81	3.80	1.06	1.10

DOI: 10.1021/acs.jpcc.8b09371
J. Phys. Chem. C 2018, 122, 26298−26306

is an active quenching mechanism in the 1%-doped NCs and that shell growth is effective in reducing the losses for all emitting levels. This is consistent with previous reports.[36−38] The role of ET and concentration quenching processes is quantified in the 2nd to 4th row where ratios of emission lifetimes for core−shell NCs are tabulated for different doping concentrations. Shell growth limits surface quenching, and the ratios reflect the role of quenching processes inside the NC core. The ratio of emission lifetimes in the core−shell NCs with 1 and 10% Er^{3+} is the highest for the $^4S_{3/2}$ level (3.49 vs 1.06−1.44 for other levels). This is explained by efficient $^4S_{3/2}$ cross-relaxation quenching between Er^{3+} neighbors that is effective at moderate Er^{3+} concentrations, well below the percolation point for energy migration. The ratio of the lifetimes for the 1/60% core−shell samples provides insight into the role of long-distance energy migration. The relatively large value for the $^4I_{11/2}$ emission (3.12 vs ∼1.3 for the $^4F_{9/2}$ and $^4I_{13/2}$ levels) shows that energy migration to quenching sites (possibly OH^-) is important for quenching of the $^4I_{11/2}$ emission in 60% Er^{3+}-doped NCs. The fourth row gives the ratio of lifetimes in 10% over 60% Er^{3+}-doped core−shell NCs and signifies the role of (long-range) energy migration vs (short range) cross-relaxation ET quenching. The high number for the $^4I_{11/2}$ level reflects that for this level, quenching through energy migration is important whereas for the $^4S_{3/2}$ level, short-range cross-relaxation is the dominant quenching process. For the $^4F_{9/2}$ and $^4I_{13/2}$ levels, the lifetime ratios in the core−shell NCs are between 1.1 and 1.4 for all Er^{3+} concentrations as quenching processes in the NC core are inefficient. Both the $^4F_{9/2}$ and $^4I_{13/2}$ levels are efficiently luminescing up to high Er^{3+} concentrations for core−shell NCs. Finally, in the fifth row, the ratios of the radiative decay time and the decay time in 1%-doped core−shell NCs are tabulated. The intrinsic radiative lifetime τ_0 is determined taking into account the correction for local field effects[39−42] (see the SI for details). The ratio of the radiative and observed lifetimes is the highest for the $^4I_{11/2}$ state (3.8), more than twice the ratios obtained for the $^4S_{3/2}$, $^4F_{9/2}$, and $^4I_{13/2}$ states. The relative strong quenching of the $^4I_{11/2}$ emission in low-doped core−shell NCs has been observed before and was attributed to efficient quenching by O−H vibrations resonant with the $^4I_{11/2}$ to $^4I_{13/2}$ energy gap.[38,43] Recently, confirmation for this hypothesis was reported: $NaYF_4$:Er,Yb NCs with superior UC QYs, close to the highest QYs obtained in bulk $NaYF_4$:Er,Yb, were realized by using a synthesis method in which all reactants containing OH groups (such as water and MeOH) were excluded.[44]

The present results on lifetime ratios in $NaYF_4$ core−shell NCs with 1, 10, and 60% Er^{3+} reveal that emission from the $^4I_{11/2}$ and the $^4S_{3/2}$ levels is strongly quenched at higher Er^{3+} concentrations, in spite of an inert $NaYF_4$ shell. The $^4I_{11/2}$ emission is sensitive to quenching sites inside the core that can be effectively reached by energy migration at elevated Er^{3+} concentrations. This will give rise to a significant reduction of UC efficiency, especially for the highest dopant concentration (60% Er^{3+}) at low excitation densities. Because of the resonance of the Er^{3+} $^4I_{11/2}$ and Yb^{3+} $^2F_{5/2}$ levels, energy migration to defect sites in co-doped Yb^{3+}−Er^{3+} NCs with a high total Yb + Er concentration can also lead to strongly reduced UC efficiencies. Emission from the $^4S_{3/2}$ level is quenched by effective cross-relaxation, already at Er^{3+} concentration of 10%. Emission from the $^4F_{9/2}$ and $^4I_{13/2}$ levels remains efficient (QY > 50%) up to the highest Er^{3+} concentration (60%) in core−shell NCs. This also indicates that IR (1.5 μm)-to-NIR (1000 nm) UC from the $^4I_{13/2}$ level can be more efficient than the more commonly used IR (980 nm)-to-visible (545 nm) UC.[25]

Luminescence Decay Dynamics for Yb^{3+} IR-Emitting Level. To further understand and optimize the UC efficiency in highly doped core−shell NCs under low excitation densities, also lifetime measurements were done for Yb^{3+}-doped NCs. The Yb^{3+} ion has a single ($^2F_{5/2}$) excited state and is commonly used as a sensitizer to realize brighter UC emission. Energy transfer from Yb^{3+} to Er^{3+} feeds the UC emission, and it has been established that UC QYs correlate with the lifetime of the Yb^{3+} excited state.[37] Faster relaxation of the Yb^{3+} emission through energy migration to quenching sites reduces the UC efficiency. Modeling of energy migration is complex, but rate equation models have been able to reproduce excited-state dynamics in concentrated UC NCs.[37] In Figure S3, $^2F_{5/2}$ emission decay curves are displayed as a function of Yb^{3+} concentration for $NaYF_4$:*X*% Yb^{3+} core-only NCs (*X* = 1−100). The lifetime shortens with increasing Yb^{3+} concentration, which can be explained by concentration quenching related to energy migration to surface quenching sites at elevated Yb^{3+} concentrations. To investigate the influence of shell growth, Figure 4 displays the luminescence decay curves for the Yb^{3+}

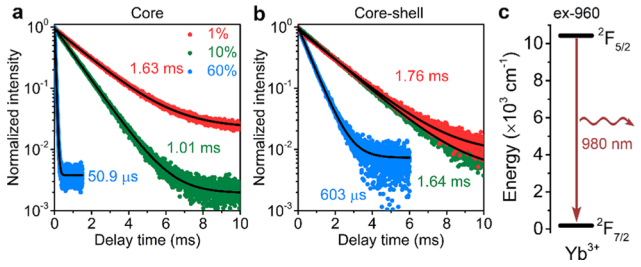

Figure 4. Luminescence decay curves of Yb^{3+} $^2F_{5/2}$ emission for direct excitation at 960 nm for (a) $NaYF_4$:*X*% Yb^{3+} core and (b) $NaYF_4$:*X*% Yb^{3+}@$NaYF_4$ core−shell NCs (*X* = 1, 10, 60 in red, green, and blue color) and (c) corresponding energy-level diagram.

emission in core-only and core−shell $NaYF_4$ NCs with 1, 10, and 60% Yb^{3+}. The lifetime ratios are also included in Table 1. For core-only NCs, a rapid decrease in lifetime is observed, especially in the 60%-doped NC. After shell growth, $^2F_{5/2}$ emission decay time is similar for the 1 and 10% doped NCs and close to the radiative decay time (1.93 ms, see the SI for details). Upon doping with 60%, the decay time drops to 603 μs corresponding to a QY of ∼30%. The high efficiency and limited quenching of the Yb^{3+} $^2F_{5/2}$ emission can be understood from the large energy separation (∼10 000 cm^{-1}) between $^2F_{5/2}$ excited state and $^2F_{7/2}$ ground state which limits multiphonon relaxation. The present results indicate that in spite of this large gap, concentration quenching does occur at concentrations above 10%, which can cause a reduction in UC efficiency at low excitation densities in highly Yb^{3+}-doped NCs reported in the literature.[45,46] Optimizing the Er concentration to enhance the Yb^{3+}−Er^{3+} energy transfer rate can provide a more efficient competing UC channel and reduce the role of concentration quenching. Indeed, in a recent study, it was found that for low excitation powers in concentrated Yb NCs ($NaYb_{1-x}Er_xF_4$), the optimum Er concentration is 8% (*x* = 0.08), significantly higher than the typically used Er^{3+} concentration of 2%.[15]

DOI: 10.1021/acs.jpcc.8b09371
J. Phys. Chem. C 2018, 122, 26298−26306

Solvent Quenching for UC NCs. *Er^{3+} IR-Emitting Levels.* In addition to dopant concentration, also the solvents in which the NCs are dispersed affect the UC efficiency. In a recent paper,[23] Plwe demonstrated how by coupling with high-energy vibrations of surrounding solvent molecules, the various energy levels involved in the UC process are quenched. Shell growth strongly reduces the quenching by increasing the distance between the optically active centers and the high-energy vibrations.[22,23] To further understand the role of solvent quenching, the luminescence decay dynamics of Er^{3+} and Yb^{3+} states were investigated for $NaYF_4$:1% Er^{3+}@$NaYF_4$ and $NaYF_4$:1% Yb^{3+}@$NaYF_4$ core−shell NCs in three solvents: cyclohexane (with 2900−3000 cm^{-1} of C−H vibrations from surrounding solvent molecules and surface ligands), H_2O (3200−3700 cm^{-1} of O−H vibrations), and heavy water D_2O (chemically the same as water but with much lower vibrational energies 2200−2500 cm^{-1} for O−D vibrations). Low doping concentrations were used to prevent interference with concentration quenching. Hydrophobic NCs passivated with oleate ligands are dispersed in cyclohexane. Acid treatment (see the SI for details) removes the oleate ligands and allows NCs to dissolve in deionized water H_2O and heavy water D_2O.[47,48] Figure 5a,b shows the decay curves of IR $^4I_{11/2}$ and $^4I_{13/2}$ emission for $NaYF_4$:1% Er^{3+}@$NaYF_4$ core−shell NCs in the three solvents. The decay time decreases in the order of D_2O, cyclohexane, and H_2O. When considering the influence of local field effects (n(cyclohexane) = 1.43 and $n(H_2O/D_2O)$ = 1.33), the radiative lifetimes are 8.54 and 10.26 ms for $^4I_{11/2}$ emission in cyclohexane and H_2O/D_2O and 9.06 and 11.01 ms for $^4I_{13/2}$ emission in cyclohexane and H_2O/D_2O, respectively.

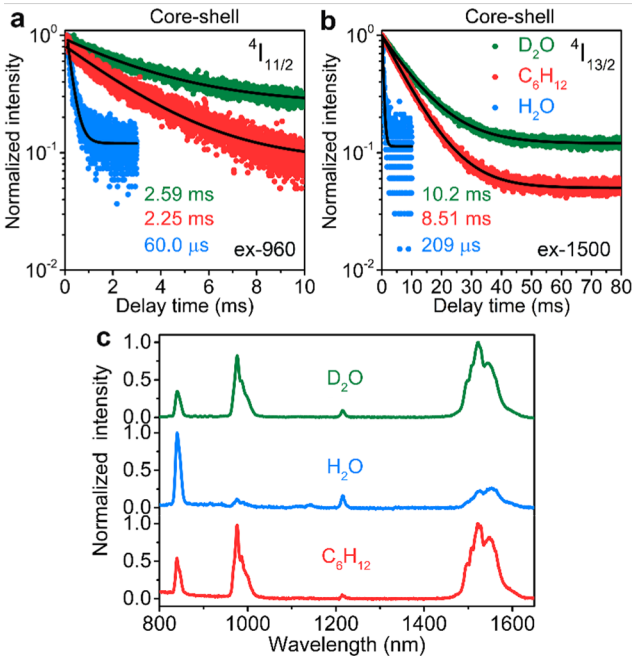

Figure 5. Luminescence decay curves of (a) Er^{3+} $^4I_{11/2}$ and (b) $^4I_{13/2}$ emission by direct excitations of 960 and 1500 nm and (c) emission spectra of 520 nm excitation for $NaYF_4$:1% Er^{3+}@$NaYF_4$ core−shell NCs in heavy water, cyclohexane, and deionized water.

The lifetimes observed for the $^4I_{11/2}$ and $^4I_{13/2}$ emission are similar for the NCs in cyclohexane and D_2O, indicating similar QY for IR emission in the two solvents. For the $^4I_{13/2}$ level, the lifetimes in the core−shell NCs are close to the radiative lifetimes in D_2O and cyclohexane. The energy gap to the ground state of ∼6500 cm^{-1} requires more than two vibrations in D_2O and cyclohexane, and clearly the three-phonon relaxation rate for the Er^{3+} ions in core−shell NCs is much lower than the radiative decay rate and the efficiency of the $^4I_{13/2}$ level is close to 100% in cyclohexane and D_2O. For the NCs in water, the two-vibrational overtone of the O−H vibrations is resonant with the 6500 cm^{-1} energy gap. Even with the 5 nm protective shell, two-phonon relaxation can compete with radiative decay, giving rise to a faster (209 μs) decay of the $^4I_{13/2}$ emission in H_2O. The $^4I_{11/2}$−$^4I_{13/2}$ energy gap of ∼3500 cm^{-1} is small enough to allow the two-phonon relaxation process in D_2O and cyclohexane, and this gives rise to a shortening of the lifetime to 2.2−2.6 ms for the $^4I_{11/2}$ emission of Er^{3+} in the core−shell NCs (radiative decay time 8.54 ms). As a single O−H vibration can bridge the energy gap to the $^4I_{13/2}$ level, the $^4I_{11/2}$ emission is very sensitive to the presence of O−H vibrations. In H_2O, the emission decay time is 60 μs and the $^4I_{11/2}$ emission is strongly quenched by phonon relaxation, in spite of the 5 nm inert shell. The sensitivity to water is further illustrated in Figure S4 where the $^4I_{11/2}$ decay dynamics is shown for gradual H_2O addition to $NaYF_4$:1% Er^{3+}@$NaYF_4$ core−shell NCs in D_2O. For small amounts of H_2O, strong quenching of the $^4I_{11/2}$ emission is observed. The emission spectra upon excitation in the $^2H_{11/2}$ level at 520 nm shown in Figure 5c provide further evidence for the solvent effect. Taking the $^4S_{3/2}$−$^4I_{13/2}$/$^4I_{9/2}$−$^4I_{15/2}$ emission at 840 nm as a reference, the emission at 976 and 1522 nm ($^4I_{11/2}$, $^4I_{13/2}$ → $^4I_{15/2}$) is strongly quenched in H_2O but is equally strong for the NCs in D_2O and cyclohexane.

Er^{3+} Vis-Emitting Levels. We also investigated the role of vibrationally induced quenching in water for the visible UC emission (Figure S5). The emission lifetimes are similar for the $^4S_{3/2}$ and $^4F_{9/2}$ levels in cyclohexane and D_2O (436 and 471 μs for the $^4S_{3/2}$ level and 325 and 379 μs for the $^4F_{9/2}$ level). In H_2O, the lifetimes become faster (241 and 262 μs for $^4S_{3/2}$ and $^4F_{9/2}$ emission). The decrease in lifetime by changing the solvent from D_2O to H_2O is 49% for the $^4S_{3/2}$ emission and 31% for the $^4F_{9/2}$ emission. The fact that the O−H vibrational energy is closer in resonance to the energy separation between $^4S_{3/2}$ and $^4F_{9/2}$ states (∼3200 cm^{-1}) than for $^4F_{9/2}$ to $^4I_{9/2}$ energy gap (∼2800 cm^{-1}) can explain the stronger quenching for $^4S_{3/2}$ state in H_2O. This result is in agreement with the observation that changing to H_2O as solvent can enhance red emission at the expense of green emission upon a 980 nm excitation.[47] Previously, an unexpected longer lifetime for red $^4F_{9/2}$ emission was reported for Er^{3+}-doped NCs in H_2O compared to that for D_2O under 380 nm excitation in the $^4G_{11/2}$ state.[49] This was interpreted as an increased $^4F_{9/2}$ population through multiphonon relaxation from higher-energy levels. Here, lifetime measurement under direct excitation (Figure S5b) clearly demonstrates more pronounced quenching for the red-emitting $^4F_{9/2}$ level by O−H vibrations (emission lifetime 262 μs) in comparison to O−D vibrations (379 μs), in line with what is expected based on higher vibrational energy of O−H vibrations. Note that all experiments for solvent quenching were conducted on core−shell NCs. Much stronger vibrational quenching is observed for core-only NCs.

The present analysis of luminescence decay times under direct excitation for various energy levels of Er^{3+} in core−shell

DOI: 10.1021/acs.jpcc.8b09371
J. Phys. Chem. C 2018, 122, 26298−26306

NCs dispersed in different solvents reveals a clear difference for the role of the high-energy O−H vibrations of water. Both IR levels ($^4I_{11/2}$ and $^4I_{13/2}$) that serve as intermediate levels in UC processes show significant quenching by ET to the high-energy O−H vibrations, even in core−shell NCs. The presently used shell thickness of 5 nm is not sufficient to protect the IR-emitting levels from quenching by ET to the fundamental O−H vibration (3500 cm^{-1}) for the $^4I_{11/2}$ level or the two-phonon mode for the $^4I_{13/2}$ level. The reason for the strong quenching is a combination of a high oscillator strength for O−H vibrations (favoring ET as the Förster-type ET rate is proportional to the acceptor oscillator strength) and a long radiative lifetime for the IR-emitting levels (∼8 ms), which makes it harder for the slow radiative decay to compete with ET. To enhance UC efficiencies in aqueous media, a thicker inert shell will be beneficial. For the visible UC emission in the green and red spectral region, the transition from apolar aliphatic solvents to water induces additional nonradiative decay but the effect is less than a factor of 2.

Yb^{3+} IR-Emitting Level. In Er^{3+},Yb^{3+} co-doped UC NCs, quenching of the 980 nm NIR emission from Yb^{3+} in different solvents is known to reduce the UC efficiency. To investigate the role of Yb^{3+} concentration quenching, we measured the solvent dependence of $^2F_{5/2}$ decay for singly doped $NaYF_4$:1% Yb^{3+}@$NaYF_4$ core−shell NCs (Figure S6). The decay times for the NIR Yb^{3+} emission are very similar independent of the solvent, indicating a limited contribution of water vibrations in quenching the ∼980 nm IR emission.[23,38,49] The absence of solvent quenching is not unexpected in view of a large energy gap between $^2F_{5/2}$ and $^2F_{7/2}$ states of 10 000 cm^{-1} that requires three-phonon relaxation in water (vs four phonons in organic solvents). For the core−shell NCs, the minimum distance of 5 nm imposed by the inert shell is sufficient to virtually eliminate multiphonon quenching. The small decrease in the luminescence decay time of the $^2F_{5/2}$ emission from 2.10 in D_2O to 1.98 ms in H_2O can be ascribed to some multiphonon quenching in H_2O, and the quenching rate can be estimated to be ∼30 s^{-1}. Note that water quenching is present in core-only NCs,[43] Yb^{3+} complexes,[50] and silica-encapsulated NCs,[49] where Yb^{3+} ions are directly coupled to water molecules and ligands with high-energy vibrational modes. However, doping in crystalline dielectric media with a 5 nm shell passivation gives rise to efficient Yb^{3+} emission and sensitization of ET UC. The quenching of 980 nm NIR emission in Er^{3+},Yb^{3+} co-doped NCs in water is primarily due to rapid ET between the $^2F_{5/2}$ level of Yb^{3+} and the resonant $^4I_{11/2}$ level of Er^{3+} and quenching of the $^4I_{11/2}$ level by O−H vibrations, as discussed above.

CONCLUSIONS

There is a trend toward higher doping concentrations for both Yb^{3+} and Er^{3+} to achieve higher brightness of UC NCs. High brightness and superior quantum yields of UC emission have been reported under high power density excitation for these highly doped NCs. Insight into concentration and solvent quenching processes is however lacking and requires studies at low excitation powers where UC rates are low and decay dynamics is dominated by nonradiative and radiative decay rates of excited states. Here, we have presented a systematic investigation of decay dynamics for Er^{3+} and Yb^{3+} in core and core−shell NCs under direct excitation in various emitting levels involved in UC processes for a wide range of concentrations (1−100% doping).

Core-only NCs suffer from strong concentration quenching. Fast migration to surface ions that are strongly quenched by vibrational coupling with nearby high-energy vibrations of solvent and capping molecules can explain the pronounced concentration quenching. For core−shell NCs, surface quenching is suppressed but still concentration quenching is observed. A detailed analysis on decay behavior following direct excitation in the emitting levels demonstrates that both the $^4S_{3/2}$ (green) and $^4I_{11/2}$ (NIR) levels are strongly quenched upon raising the Er^{3+} concentration. For the $^4S_{3/2}$ level, cross-relaxation has been identified as the main quenching mechanism, whereas for the $^4I_{11/2}$ level, energy migration to defects/impurities in the core (possibly OH^-) is responsible for the observed concentration quenching. The IR-emitting $^4I_{13/2}$ and the red-emitting $^4F_{9/2}$ levels do not show strong concentration quenching, and their emission remains efficient up to high (60%) doping concentrations in core−shell NCs. Also for Yb^{3+}, limited quenching is observed in highly (60%) Yb^{3+}-doped core−shell NCs.

The role of solvent vibrations was investigated by studying decay dynamics for emission from various levels of Er^{3+} and for the NIR emission of Yb^{3+} in core−shell NCs. The results show a much stronger quenching for the IR-emitting levels $^4I_{11/2}$ and $^4I_{13/2}$ (intermediate levels in the UC process) than for the $^4S_{3/2}$ and $^4F_{9/2}$ levels responsible for the green and red UC emission. Our work provides a better understanding and deeper insight on quenching pathways in highly doped UC NCs and provides important information on design rules for efficient UC under lower power densities that are required in many applications.

ASSOCIATED CONTENT

Supporting Information

The Supporting Information is available free of charge on the ACS Publications website at DOI: 10.1021/acs.jpcc.8b09371.

Experimental methods, TEM images, ICP results, luminescence decay curves, average lifetimes, and transition probability calculation (PDF)

AUTHOR INFORMATION

Corresponding Author

*E-mail: A.Meijerink@uu.nl.

ORCID

Andries Meijerink: 0000-0003-3573-9289

Notes

The authors declare no competing financial interest.

ACKNOWLEDGMENTS

Thanks to J. C. van der Bok for helping ICP measurement and F. T. Rabouw and P. Villanueva-Delgado for the useful discussion. This work was financially supported by the China Scholarship Council (No. 201506380101).

REFERENCES

(1) Zheng, W.; Huang, P.; Tu, D. T.; Ma, E.; Zhu, H. M.; Chen, X. Y. Lanthanide-Doped Upconversion Nano-Bioprobes: Electronic Structures, Optical Properties, and Biodetection. *Chem. Soc. Rev.* **2015**, *44*, 1379−1415.

(2) Goldschmidt, J. C.; Fischer, S. Upconversion for Photovoltaics - a Review of Materials, Devices and Concepts for Performance Enhancement. *Adv. Opt. Mater.* **2015**, *3*, 510−535.

DOI: 10.1021/acs.jpcc.8b09371
J. Phys. Chem. C 2018, 122, 26298−26306

(3) Wang, F.; Liu, X. G. Recent Advances in the Chemistry of Lanthanide-Doped Upconversion Nanocrystals. *Chem. Soc. Rev.* **2009**, *38*, 976−989.
(4) Wang, X. D.; Valiev, R. R.; Ohulchanskyy, T. Y.; Ågren, H.; Yang, C. H.; Chen, G. Y. Dye-Sensitized Lanthanide-Doped Upconversion Nanoparticles. *Chem. Soc. Rev.* **2017**, *46*, 4150−4167.
(5) Wang, F.; Han, Y.; Lim, C. S.; Lu, Y. H.; Wang, J.; Xu, J.; Chen, H. Y.; Zhang, C.; Hong, M. H.; Liu, X. G. Simultaneous Phase and Size Control of Upconversion Nanocrystals through Lanthanide Doping. *Nature* **2010**, *463*, 1061−1065.
(6) Boyer, J.-C.; Cuccia, L. A.; Capobianco, J. A. Synthesis of Colloidal Upconverting $NaYF_4$: Er^{3+}/Yb^{3+} and Tm^{3+}/Yb^{3+} Monodisperse Nanocrystals. *Nano Lett.* **2007**, *7*, 847−852.
(7) Wang, F.; Liu, X. G. Upconversion Multicolor Fine-Tuning: Visible to Near-Infrared Emission from Lanthanide-Doped $NaYF_4$ Nanoparticles. *J. Am. Chem. Soc.* **2008**, *130*, 5642−5643.
(8) Wang, Y. F.; Liu, G. Y.; Sun, L. D.; Xiao, J. W.; Zhou, J. C.; Yan, C. H. Nd^{3+}-Sensitized Upconversion Nanophosphors: Efficient in Vivo Bioimaging Probes with Minimized Heating Effect. *ACS Nano* **2013**, *7*, 7200−7206.
(9) Liu, X. G.; Yan, C. H.; Capobianco, J. A. Photon Upconversion Nanomaterials. *Chem. Soc. Rev.* **2015**, *44*, 1299−1301.
(10) Zhou, J.; Liu, Z.; Li, F. Y. Upconversion Nanophosphors for Small-Animal Imaging. *Chem. Soc. Rev.* **2012**, *41*, 1323−1349.
(11) Choi, B.; Iwanaga, M.; Sugimoto, Y.; Sakoda, K.; Miyazaki, H. T. Selective Plasmonic Enhancement of Electric- and Magnetic-Dipole Radiations of Er Ions. *Nano Lett.* **2016**, *16*, 5191−5196.
(12) Han, S. Y.; Deng, R. R.; Xie, X. J.; Liu, X. G. Enhancing Luminescence in Lanthanide-Doped Upconversion Nanoparticles. *Angew. Chem., Int. Ed.* **2014**, *53*, 11702−11715.
(13) Zhao, J. B.; Jin, D. Y.; Schartner, E. P.; Lu, Y. Q.; Liu, Y. J.; Zvyagin, A. V.; Zhang, L. X.; Dawes, J. M.; Xi, P.; Piper, J. A.; Goldys, E. M.; Monro, T. M. Single-Nanocrystal Sensitivity Achieved by Enhanced Upconversion Luminescence. *Nat. Nanotechnol.* **2013**, *8*, 729−734.
(14) Gargas, D. J.; Chan, E. M.; Ostrowski, A. D.; Aloni, S.; Altoe, M. V. P.; Barnard, E. S.; Sanii, B.; Urban, J. J.; Milliron, D. J.; Cohen, B. E.; et al. Engineering Bright Sub-10-nm Upconverting Nanocrystals for Single-Molecule Imaging. *Nat. Nanotechnol.* **2014**, *9*, 300−305.
(15) Liu, Q.; Zhang, Y. X.; Peng, C. S.; Yang, T.; Joubert, L.-M.; Chu, S. Single Upconversion Nanoparticle Imaging at Sub-10 W cm^{-2} Irradiance. *Nat. Photonics* **2018**, *12*, 548−553.
(16) Tian, B. N.; Fernandez-Bravo, A.; Najafiaghdam, H.; Torquato, N. A.; Altoe, M. V. P.; Teitelboim, A.; Tajon, C. A.; Tian, Y.; Borys, N. J.; Barnard, E. S.; et al. Low Irradiance Multiphoton Imaging with Alloyed Lanthanide Nanocrystals. *Nat. Commun.* **2018**, *9*, No. 3082.
(17) Haase, M.; Schäfer, H. Upconverting Nanoparticles. *Angew. Chem., Int. Ed.* **2011**, *50*, 5808−5829.
(18) Boyer, J.-C.; van Veggel, F. C. J. M. Absolute Quantum Yield Measurements of Colloidal $NaYF_4$: Er^{3+}, Yb^{3+} Upconverting Nanoparticles. *Nanoscale* **2010**, *2*, 1417−1419.
(19) Zhang, F.; Che, R. C.; Li, X. M.; Yao, C.; Yang, J. P.; Shen, D. K.; Hu, P.; Li, W.; Zhao, D. Y. Direct Imaging the Upconversion Nanocrystal Core/Shell Structure at the Subnanometer Level: Shell Thickness Dependence in Upconverting Optical Properties. *Nano Lett.* **2012**, *12*, 2852−2858.
(20) Li, D. H.; Liu, X. F.; Qiu, J. R. Probing Interaction Distance of Surface Quenchers in Lanthanide-Doped Upconversion Core-Shell Nanoparticles. *J. Phys. Chem. C* **2018**, *122*, 10278−10283.
(21) Yi, G.-S.; Chow, G.-M. Water-Soluble $NaYF_4$:Yb,Er(Tm)/$NaYF_4$/Polymer Core/Shell/Shell Nanoparticles with Significant Enhancement of Upconversion Fluorescence. *Chem. Mater.* **2007**, *19*, 341−343.
(22) Fischer, S.; Bronstein, N. D.; Swabeck, J. K.; Chan, E. M.; Alivisatos, A. P. Precise Tuning of Surface Quenching for Luminescence Enhancement in Core-Shell Lanthanide-Doped Nanocrystals. *Nano Lett.* **2016**, *16*, 7241−7247.
(23) Rabouw, F. T.; Prins, P. T.; Villanueva-Delgado, P.; Castelijns, M.; Geitenbeek, R. G.; Meijerink, A. Quenching Pathways in $NaYF_4$:Er^{3+},Yb^{3+} Upconversion Nanocrystals. *ACS Nano* **2018**, *12*, 4812−4823.
(24) Vetrone, F.; Boyer, J.-C.; Capobianco, J. A.; Speghini, A.; Bettinelli, M. Concentration-Dependent Near-Infrared to Visible Upconversion in Nanocrystalline and Bulk Y_2O_3:Er^{3+}. *Chem. Mater.* **2003**, *15*, 2737−2743.
(25) Martín-Rodríguez, R.; Rabouw, F. T.; Trevisani, M.; Bettinelli, M.; Meijerink, A. Upconversion Dynamics in Er^{3+}-Doped Gd_2O_2S: Influence of Excitation Power, Er^{3+} Concentration, and Defects. *Adv. Opt. Mater.* **2015**, *3*, 558−567.
(26) Vetrone, F.; Boyer, J.-C.; Capobianco, J. A.; Speghini, A.; Bettinelli, M. Significance of Yb^{3+} Concentration on the Upconversion Mechanisms in Codoped Y_2O_3:Er^{3+}, Yb^{3+} Nanocrystals. *J. Appl. Phys.* **2004**, *96*, 661−667.
(27) Chan, E. M.; Levy, E. S.; Cohen, B. E. Rationally Designed Energy Transfer in Upconverting Nanoparticles. *Adv. Mater.* **2015**, *27*, 5753−5761.
(28) Su, Q. Q.; Han, S. Y.; Xie, X. J.; Zhu, H. M.; Chen, H. Y.; Chen, C. K.; Liu, R. S.; Chen, X. Y.; Wang, F.; Liu, X. G. The Effect of Surface Coating on Energy Migration-Mediated Upconversion. *J. Am. Chem. Soc.* **2012**, *134*, 20849−20857.
(29) Shalav, A.; Richards, B. S.; Trupke, T.; Krämer, K. W.; Güdel, H. U. Application of $NaYF_4$:Er^{3+} Up-Converting Phosphors for Enhanced Near-Infrared Silicon Solar Cell Response. *Appl. Phys. Lett.* **2005**, *86*, No. 013505.
(30) Yan, R. X.; Li, Y. D. Down/Up Conversion in Ln^{3+}-Doped YF_3 Nanocrystals. *Adv. Funct. Mater.* **2005**, *15*, 763−770.
(31) Krämer, K. W. Resonance in Er^{3+} Upconversion Excitation. *J. Lumin.* **2017**, *189*, 78−83.
(32) Auzel, F. Upconversion and Anti-Stokes Processes with f and d Ions in Solids. *Chem. Rev.* **2004**, *104*, 139−173.
(33) Johnson, N. J. J.; He, S.; Diao, S.; Chan, E. M.; Dai, H. J.; Almutairi, A. Direct Evidence for Coupled Surface and Concentration Quenching Dynamics in Lanthanide-Doped Nanocrystals. *J. Am. Chem. Soc.* **2017**, *139*, 3275−3282.
(34) Schietinger, S.; Menezes, L. d. S.; Lauritzen, B.; Benson, O. Observation of Size Dependence in Multicolor Upconversion in Single Yb^{3+}, Er^{3+} Codoped $NaYF_4$ Nanocrystals. *Nano Lett.* **2009**, *9*, 2477−2481.
(35) Capobianco, J. A.; Vetrone, F.; D'Alesio, T.; Tessari, G.; Speghini, A.; Bettinelli, M. Optical Spectroscopy of Nanocrystalline Cubic Y_2O_3:Er^{3+} Obtained by Combustion Synthesis. *Phys. Chem. Chem. Phys.* **2000**, *2*, 3203−3207.
(36) Hebbink, G. A.; Stouwdam, J. W.; Reinhoudt, D. N.; van Veggel, F. C. J. M. Lanthanide(III)-Doped Nanoparticles That Emit in the Near-Infrared. *Adv. Mater.* **2002**, *14*, 1147−1150.
(37) Hossan, M. Y.; Hor, A.; Luu, Q.; Smith, S. J.; May, P. S.; Berry, M. T. J. Explaining the Nanoscale Effect in the Upconversion Dynamics of β-$NaYF_4$:Yb^{3+}, Er^{3+} Core and Core-Shell Nanocrystals. *J. Phys. Chem. C* **2017**, *121*, 16592−16606.
(38) Wang, F.; Wang, J.; Liu, X. G. Direct Evidence of a Surface Quenching Effect on Size-Dependent Luminescence of Upconversion Nanoparticles. *Angew. Chem., Int. Ed.* **2010**, *49*, 7456−7460.
(39) Toptygin, D. Effects of the Solvent Refractive Index and Its Dispersion on the Radiative Decay Rate and Extinction Coefficient of a Fluorescent Solute. *J. Fluoresc.* **2003**, *13*, 201−219.
(40) Rabouw, F. T.; den Hartog, S. A.; Senden, T.; Meijerink, A. Photonic Effects on the Förster Resonance Energy Transfer Efficiency. *Nat. Commun.* **2014**, *5*, No. 3610.
(41) Senden, T.; Rabouw, F. T.; Meijerink, A. Photonic Effects on the Radiative Decay Rate and Luminescence Quantum Yield of Doped Nanocrystals. *ACS Nano* **2015**, *9*, 1801−1808.
(42) Wang, Z. J.; Senden, T.; Meijerink, A. Photonic Effects for Magnetic Dipole Transitions. *J. Phys. Chem. Lett.* **2017**, *8*, 5689−5694.
(43) Boyer, J. C.; Manseau, M. P.; Murray, J. I.; Van Veggel, F. C. J. M. Surface Modification of Upconverting $NaYF_4$ Nanoparticles with PEG-Phosphate Ligands for NIR (800 nm) Biolabeling within the Biological Window. *Langmuir* **2010**, *26*, 1157−1164.

DOI: 10.1021/acs.jpcc.8b09371
J. Phys. Chem. C 2018, 122, 26298−26306

(44) Homann, C.; Krukewitt, L.; Frenzel, F.; Grauel, B.; Wurth, C.; Resch-Genger, U.; Haase, M. $NaYF_4$:Yb,Er/$NaYF_4$ Core/Shell Nanocrystals with High Upconversion Quantum Yield. *Angew. Chem., Int. Ed.* **2018**, *57*, 8765−8769.
(45) Ma, C.; Xu, X. X.; Wang, F.; Zhou, Z. G.; Liu, D. M.; Zhao, J. B.; Guan, M.; Lang, C. I.; Jin, D. Y. Optimal Sensitizer Concentration in Single Upconversion Nanocrystals. *Nano Lett.* **2017**, *17*, 2858−2864.
(46) Chen, G. Y.; Ohulchanskyy, T. Y.; Kumar, R.; Agren, H.; Prasad, P. N. Ultrasmall Monodisperse $NaYF_4$:Yb^{3+}/Tm^{3+} Nanocrystals with Enhanced Near-Infrared to Near-Infrared Upconversion Photoluminescence. *ACS Nano* **2010**, *4*, 3163−3168.
(47) Bogdan, N.; Vetrone, F.; Ozin, G. A.; Capobianco, J. A. Synthesis of Ligand-Free Colloidally Stable Water Dispersible Brightly Luminescent Lanthanide-Doped Upconverting Nanoparticles. *Nano Lett.* **2011**, *11*, 835−840.
(48) Lappi, S. E.; Smith, B.; Franzen, S. Infrared Spectra of $H_2{}^{16}O$, $H_2{}^{18}O$ and D_2O in the Liquid Phase by Single-Pass Attenuated Total Internal Reflection Spectroscopy. *Spectrochim. Acta, Part A* **2004**, *60*, 2611−2619.
(49) Arppe, R.; Hyppänen, I.; Perälä, N.; Peltomaa, R.; Kaiser, M.; Würth, C.; Christ, S.; Resch-Genger, U.; Schäferling, M.; Soukka, T. Quenching of the Upconversion Luminescence of $NaYF_4$:Yb^{3+},Er^{3+} and $NaYF_4$:Yb^{3+},Tm^{3+} Nanophosphors by Water: The Role of the Sensitizer Yb^{3+} in Non-Radiative Relaxation. *Nanoscale* **2015**, *7*, 11746−11757.
(50) Moore, E. G.; Seitz, M.; Raymond, K. N. Use of Yb^{III}-Centered Near-Infrared (NIR) Luminescence to Determine the Hydration State of a 3, 2-HOPO-Based MRI Contrast Agent. *Inorg. Chem.* **2008**, *47*, 8571−8573.

DOI: 10.1021/acs.jpcc.8b09371
J. Phys. Chem. C 2018, 122, 26298−26306